46 Weglicki, W B, Mak, T and Phillips, T M, *Circ Res*, 1994, 74 1009–1013
47 Kramer J H, Misik, V and Weglicki, W B, *Free Radical Biol Med*, 1994, 16, 713–723
48 Shivakumar, K and Renuka Nair, R, *Mol Cell Biochem*, 1991, 100, 91–96

Received 24 March 1995, revised accepted 4 April 1995

RESEARCH ARTICLES

Model calculations of competing climatic effects of SO_2 and CO_2 in fossil fuel combustion

M. Rajeevan, K. C. Sinha Ray and H. N. Srivastava

India Meteorological Department, Shivajinagar, Pune 411 005, India

Fossil fuel combustion has two competing effects on the climate system, a warming due to the emission of CO_2 and other trace gases and a cooling due to sulphate particles formed from the SO_2 emission. A detailed parameterization of the relationship between fossil fuel burning and the SO_2 effect on backscattering and cloud albedo is implemented in a one-dimensional radiative–convective model for assessing the climatic impact. The results show that at present the cooling induced by the combined effect of SO_2 completely counteracts the CO_2 greenhouse warming. The model predicts that by the year 2060 the SO_2-induced cooling reduces warming due to CO_2 by 66% in the IPCC scenario BaU and by 27% in the IPCC scenario D. Attempts to slow-pace the fossil fuel burning will decrease the SO_2 concentration, which could further increase global warming.

WHEN fossil fuel is burned, both carbon dioxide and sulphur dioxide are added to the atmosphere. Carbon dioxide being a greenhouse gas has a warming effect on the climate system. The radiative effect of CO_2 is relatively easy to assess based on its infrared absorption and emission properties.

In the atmosphere, sulphur dioxide goes on to oxidize with compounds in the troposphere to produce aerosol particles. These hygroscopic submicron particles also affect our climate but in a different way. These particles scatter solar radiation back to space, causing a direct cooling – this is called the direct effect. These particles also increase the concentration of cloud condensation nuclei (CCN). An increase in the CCN concentration can cause an increase in the cloud droplet concentration, which will cause an increase in the total reflective surface area within the cloud, thus leading to an increase in the cloud albedo. This is called the indirect effect. Major difficulties in the study of climatic effect due to SO_2 emission result from the fact that the atmospheric sulphuric compounds have a short lifetime, a nonhomogeneous distribution of sources and a variable vertical distribution of concentration.

The increase and the predicted radiative forcing resulting from the four Intergovernmental Panel for Climate Change (IPCC) greenhouse gases emission scenarios were known to us. The Business-as-Usual (BaU) scenario represents a continued increase in the consumption rate of fossil fuel at the present pace. Scenarios B and C represent a lower rate of increase. Scenario D represents levelling off of the consumption rate close to the 1990 consumption rate and a decrease after the year 2010. Spatially specific projections of future climate change assumed CO_2 to be the only forcing agent in fossil fuel burning, aerosols having been ignored[1,2]. This means that projections may well be grossly in error over much of the world[3].

Charlson *et al.*[4] suggested that the direct SO_2-induced forcing is comparable but opposite to the anthropogenic CO_2-induced forcing. Recently Kiehl and Briegleb[5] and Taylor and Penner[6] calculated the direct radiative forcing due to sulphate aerosols. The indirect forcing was recently calculated by Jones *et al.*[7] At the present emission level, the SO_2-induced cooling has the potential of at least partially offsetting the CO_2-induced warming[8].

In this paper, we present a detailed analysis of the climatic effects of CO_2 and SO_2 using a one-dimensional radiative–convective model. Here we present an analysis of the relationship between fossil fuel burning, CO_2 and SO_2 emission, the concentration of anthropogenic CCN, reflected solar radiation and cloud albedo, along with a simulation of the combined SO_2 and CO_2 climatic effect.

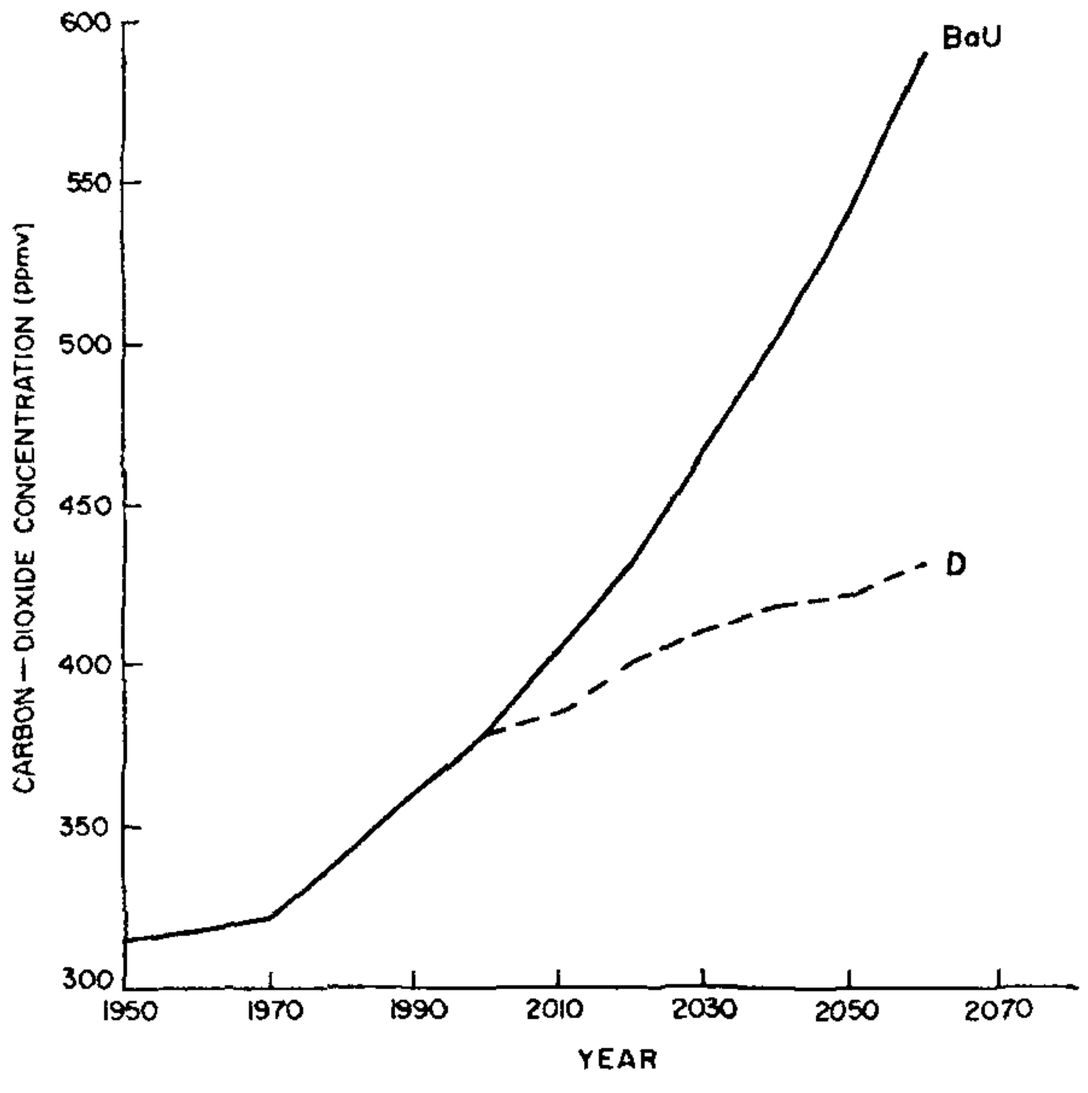

Figure 1. The atmospheric CO_2 concentrations for the IPCC scenarios BaU and D for fossil fuel consumption

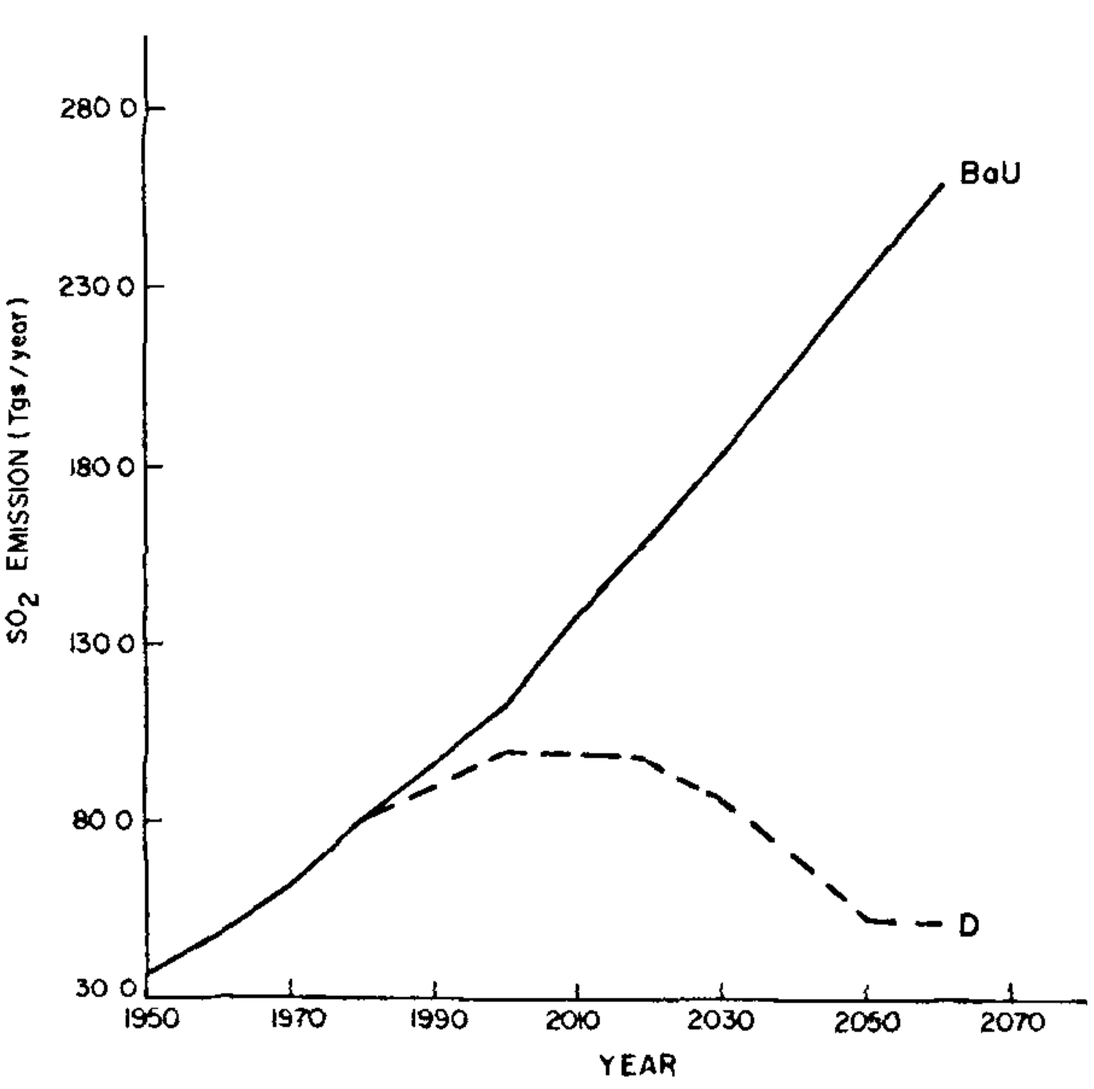

Figure 2. Anthropogenic emission rates of sulphur, based on the emission estimated by Moller[11] for the period 1950–1985 and on the future consumption rates (BaU and D) according to the IPCC report

CO_2 and SO_2 concentrations

Anthropogenic CO_2 is emitted in the atmosphere mainly by fossil fuel and biomass burning. We have used the past and anticipated CO_2 concentrations estimated by Kaufman and Chou[10] based on the consumption rates given in the IPCC Report[9]. The concentrations are shown in Figure 1. BaU scenario represents a continued increase in the consumption rate of fossil fuel at the present pace. Scenario D represents a levelling off of the consumption rate and a decrease after the year 2010.

The data on the rate of SO_2 emission, $P_s(t)$, for the period 1950–1985 were taken from Moller[11]. The data for the period after 1985 were taken from Kaufman and Chou[10], estimated using the IPCC scenarios for fossil fuel consumption. To convert the fossil fuel consumption rate into SO_2 emission rate, it is assumed that the present ratio between SO_2 emission and fossil fuel consumption remains unchanged in the future.

The future emission rate of SO_2, $P_s(t)$, is given by

$$P_s(t) = P_s(1985) \cdot P_f(t)/P_f(1985) \quad \text{for } t > 1985, \tag{1}$$

where $P_f(t)$ is the rate of fossil fuel consumption according to the IPCC scenarios and $P_f(1985)$ is the rate of fossil fuel consumption in 1985, $P_s(1985)$ is the SO_2 emission rate in 1985 taken from Moller[11]. Plots of $P_s(t)$ are shown in Figure 2.

To calculate the direct effect of aerosol particles, sulphate burden (g m^{-2}) is to be prescribed. Sulphate burden,

$$\rho_{aero}(t) = f_a \cdot P_s(t) \cdot T_s/(\alpha \cdot S), \tag{2}$$

where f_a is the fraction of sulphur that forms aerosol particles, T_s is the lifetime of sulphate particles, α is the fraction of the earth's surface area containing aerosol particles and S is the area of the earth's surface. About half the amount of sulphur dioxide is lost directly from the atmosphere, either washed out by rain or reacts chemically with plants, soil or sea water. The remainder 50% goes on to oxidize to produce aerosol particles[4]. We have, therefore, used $f_a = 0.5$. We have used $T_s = 6$ days and $\alpha = 0.26$ (ref. 4).

To calculate the indirect effect, the density (g m^{-3}) of sulphur that forms potential CCN is calculated as

$$\rho_{CCN}(t) = \rho_{aero}(t) \cdot f_c/H, \tag{3}$$

where f_c is the fraction of aerosol particles that have a potential to form cloud droplets. Kaufman and Chou[10] used $f_c = 0.4$. H is the height of aerosol layer above the surface. We have assumed $H = 2$ km.

The relationship between the concentration of anthropogenic CCN and the density of sulphur is given by

$$\Delta N_c(t) = \rho_{CCN}(t)/(\tfrac{4}{3}\pi r_m^3 d) \cdot f_{ws},$$

where r_m is the mass weighted mean radius of the sulphate aerosol particles, d the density of aerosol particles and f_{ws} the fraction of the particles weight that is composed of sulphur. We have used $f_{ws} = 0.125$, because roughly one-eighth of the total mass of CCN is sul-

phur[10], and $d = 1.5$ g cm^{-3} for sulphate particles. Therefore,

$$\Delta N_c(t) = 1.33\, \rho_{CCN}(t)/r_m^3 \ (\text{cm}^{-3}). \tag{4}$$

Whitby[12] estimated the mean value of r_m to be 1.5×10^{-5} cm.

The relationship between the cloud optical thickness and the density of cloud droplets for a constant liquid water content is given by Twomey[13]:

$$\frac{\tau(t)}{\tau_0} = \left(1 + \frac{\Delta N_c(t)}{N_{co}}\right)^{0.24}, \tag{5}$$

where the subscript 0 denotes unperturbed situations.

From equation (5) it can be seen that there is a strong nonlinearity in the relationship between the change in the cloud optical thickness and the CCN concentration. Due to this nonlinearity a constant increase in the emission rate in the future will cause a smaller forcing.

The ratio of the cloud optical thickness to the 'base' values of the year 1900, $\tau(t)/\tau(1900)$, for IPCC BaU scenario and D scenario are shown in Figure 3. Cloud optical thickness due to the short lifetime of atmospheric aerosol closely follows the emission scenarios while longer CO_2 lifetime causes a monotonous increase in the CO_2 concentration for all IPCC scenarios.

Radiative–convective model and calculation method

We have used University of Illinois multilayer radiative–convective model (UIMLRCM). This model has 26 layers from the surface to 4 hPa. The model uses detailed radiative parameterizations. Short-wave calculations are based on the two-stream delta-Eddington method[14], employing eight spectral intervals. The parameterization of water vapour is based on the work of Chou and Arking[15], ozone absorption on the work of Lacis and Hansen[16] and carbon dioxide on the work of Fouquart[17]. The optical depth and single-scattering albedo for cloud droplets are determined following Stephens[18] for non-ice clouds and Starr and Cox[19] for ice clouds.

Long-wave flux equations are based on the two-stream formula for flux equations with parameterized optical depths. Gaseous absorptions due to water vapour, carbon dioxide and ozone are considered. The parameterization of water vapour, carbon dioxide and ozone is based on the works of Chou[20], Chou and Peng[21] and Kneizys *et al.*[22], respectively.

The radiative parameterization of aerosol scattering effect is also added in the model to calculate the direct effect.

The wavelength-dependent optical depth of the aerosol is calculated from the equation

$$\tau(\lambda) = \rho_{aero}(t) \cdot \psi_{ext}(\lambda) \cdot F_n(\text{rh}),$$

where ρ_{aero} is the sulphate burden, ψ_{ext} is the wavelength-dependent extinction coefficient and F_n(rh) is the scaling factor to account for the increase in scattering due to increase in relative humidity. We have used a value of 1.7 for this as per recommendation[23]. Extinction coefficients, asymmetry parameter and single-scattering albedo were calculated using the standard Mie theory. For that we assumed the size distribution as lognormal. The geometric mean radius, r_n, was specified as equal to 0.05 μm and the geometric standard deviation was 2.0.

The aerosol-specific extinction $\psi_{ext}(\lambda)$ for a given wavelength λ was obtained from

$$\psi_{ext}(\lambda) = \frac{3}{4\rho_s} \frac{\int Q_e(\lambda, r) r^2 n(r)\, dr}{\chi_{SO_4} \int r^3 n(r)\, dr}, \tag{6}$$

where the integration is over the particle radius r, $Q_e(\lambda, r)$ is the Mie extinction efficiency, $n(r)$ is the lognormal size distribution and χ_{SO_4} is the fraction of the fine particles mass that is sulphate. We used the observed value of 1.5 g cm^{-3} for the dry particle density ρ_s and 0.6 for χ_{SO_4}.

We have used the mean cloud conditions given by Manabe and Wetherald[24]. We have, however, assumed that only low and middle-layer clouds were affected by SO_2-derived particles.

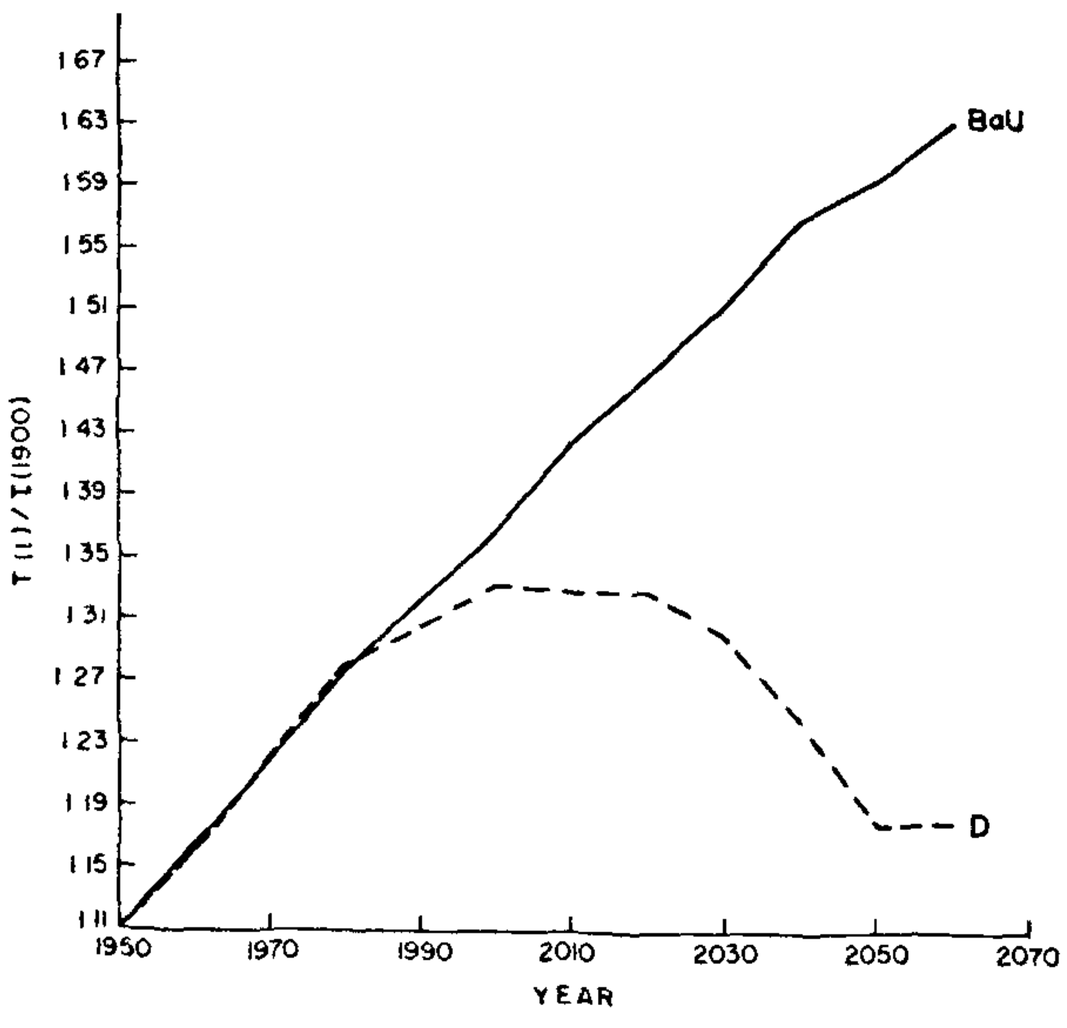

Figure 3. The ratio of cloud optical thickness to the 'base' value for the year 1900, $\tau(t)/\tau(1900)$ for the IPCC scenarios BaU and D

Climatic effects of fossil fuel burning

The climatic effects of fossil fuel burning were simulated using the radiative–convective model by

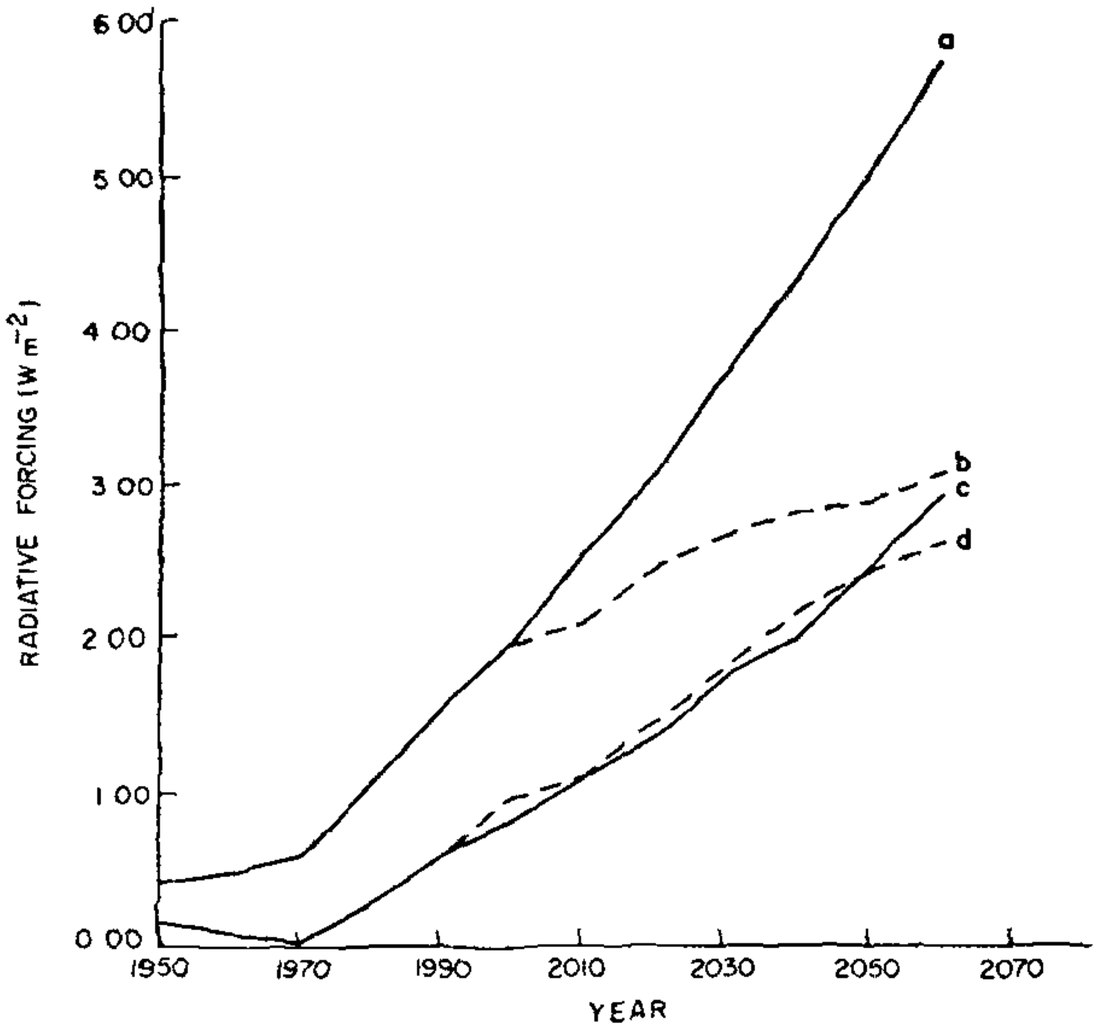

Figure 4. Radiative forcing (W m^{-2}) relative to preindustrial climate (1900) for the IPCC BaU scenario (curves a and c) and D scenario (curves b and d) Curves a and b are for CO_2 forcing and curves c and d for the combined CO_2- and SO_2-induced direct effect

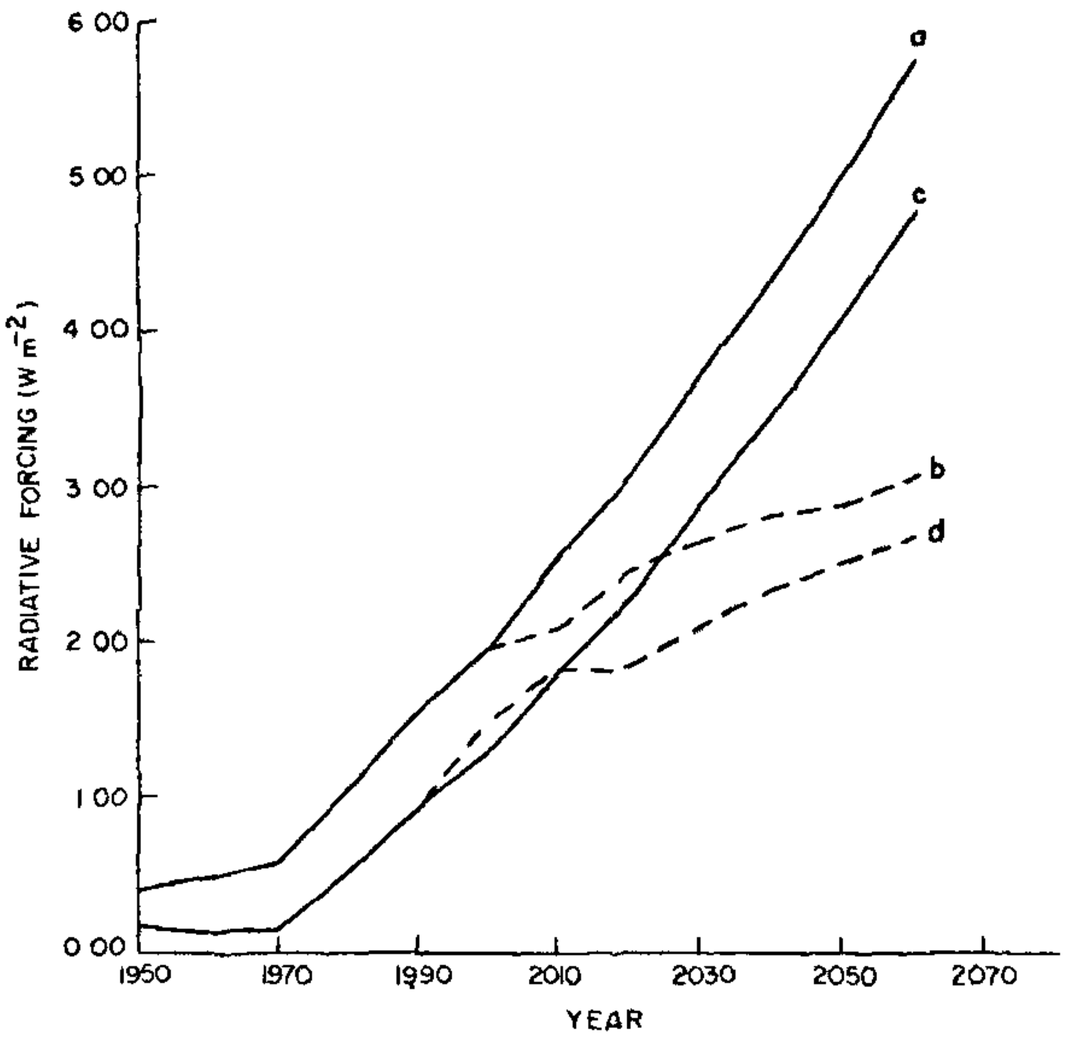

Figure 5. Radiative forcing (W m^{-2}) relative to preindustrial climate (1900) for the IPCC BaU scenario (curves a and c) and D scenario (curves b and d) Curves a and b are for CO_2 forcing and curves c and d are for the combined CO_2- and SO_2-induced indirect effect

prescribing CO_2 concentration (Figure 1), SO_2 concentration (Figure 2) and optical depth values (Figure 3) for the two extremes of IPCC scenarios. The control run was made using the CO_2 and SO_2 emission values for the year 1900. The radiative forcing at the tropopause level and the equilibrium temperatures were calculated by integrating the model forward in time with convective adjustment to maintain the critical lapse rate limit (6.5°C/km).

The radiative forcing due to CO_2 and the direct effect of SO_2 are shown in Figure 4. The radiative forcing due to CO_2 by the year 2060 is 5.74 W/m^2 for BaU scenario. By slow pace of fuel burning the effect of CO_2 is expected to reduce by about 46%. The SO_2-induced direct forcing is likely to reduce the forcing due to CO_2 in 2060 by 49% for BaU scenario and 15% for D scenario. The effect is smaller for D scenario because the atmospheric SO_2 responds to the decrease in fossil fuel consumption much faster than the CO_2 concentration. The direct radiative forcing due to SO_2 for the year 1980 is –0.78 W/m^2, which is comparable to the direct forcing of –0.9 W/m^2 calculated by Taylor and Penner[6].

The radiative forcing due to CO_2 and the indirect effect of SO_2 are shown in Figure 5. While in 1980 the SO_2-induced indirect effect reduced CO_2 forcing by about 53%, the reduction in 2060 is 17% for BaU scenario and 12% for D scenario. The smaller effect in 2060 than in 1980 results from the nonlinear dependence of the cloud optical thickness on the SO_2 concentration. In this case also, the effect is still smaller for D scenario, for the reasons mentioned earlier. The radiative forcing due to the indirect effect for the year 1990 is –0.607 W/m^2, which is comparable to that of Kaufman and Chou[10].

The radiative forcing due to CO_2 and the combined effect of SO_2 are shown in Figure 6. The negative forcing due to the direct and indirect effects of SO_2 for the year 1990 is more than the positive forcing due to CO_2, thus leading to overall cooling. By 2060 the combined effect of SO_2 is expected to reduce the CO_2 forcing by about 66% in BaU scenario and 27% in D scenario. It may be noted that the reduction of CO_2-induced forcing in D scenario is smaller than in BaU scenario. Because of the short atmospheric lifetimes of sulphate and its precursors, atmospheric concentrations will adjust within weeks to changes in emissions. This is a different situation from that of CO_2, which has an effective lifetime of decades. For example, the concentrations of CO_2 will continue to increase for more than a century even if emissions are kept constant at present-day level.

Figure 7 shows the equilibrium temperatures calculated in the model simulations for CO_2 and SO_2 concentrations. The results are similar to those for radiative forcing (Figure 6). It is expected that by 2060, SO_2-induced cooling will reduce the CO_2-induced warming of 1.61°C to 0.43°C. In general, it is also expected that SO_2-induced direct effect is likely to counteract CO_2-induced warming more efficiently than the indirect effect.

Discussion

It is concluded that the emission of SO_2 for BaU scenario has a potential of offsetting the CO_2-induced

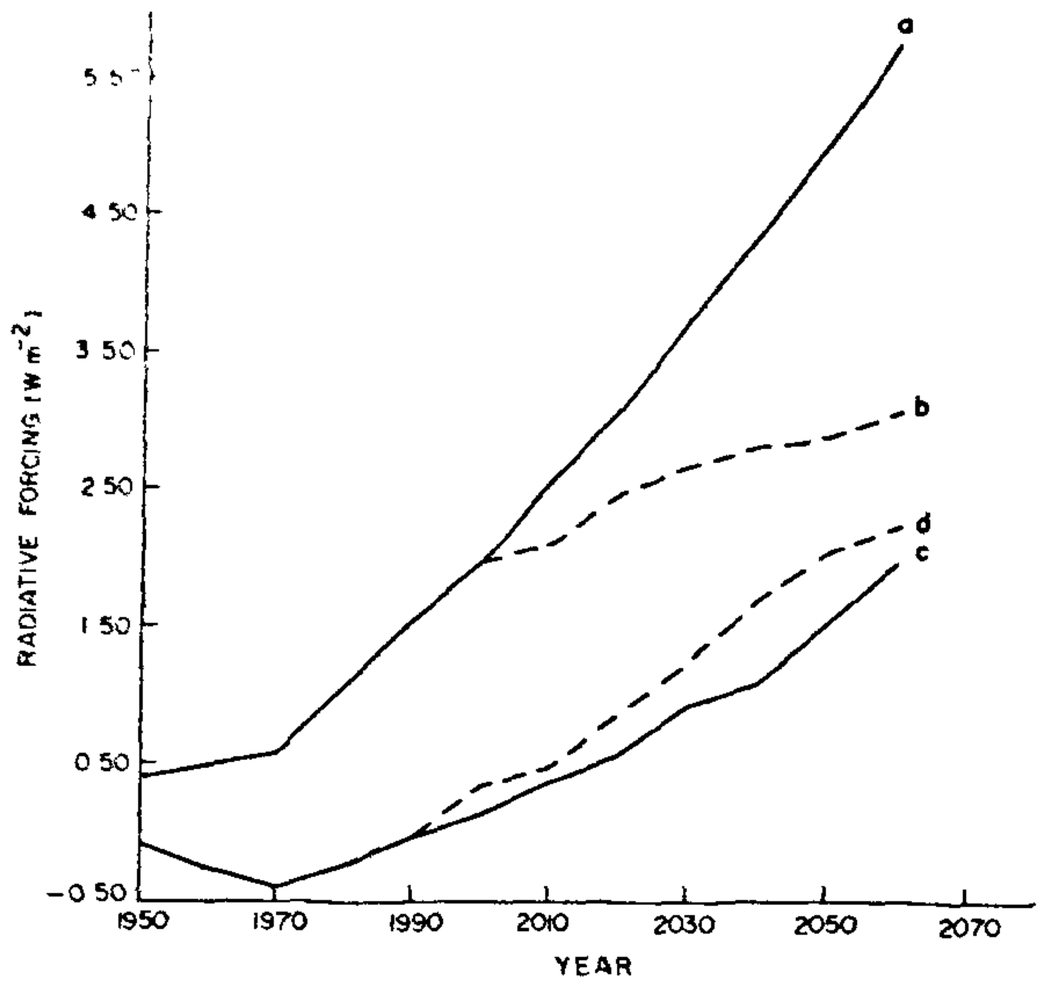

Figure 6. Radiative forcing (W m^{-2}) relative to preindustrial climate (1900) for the IPCC BaU scenario (curves a and c) and D scenario (curves b and d) Curves a and b are for CO_2 forcing and curves c and d are for the combined CO_2- and SO_2-induced total (direct and indirect) effect

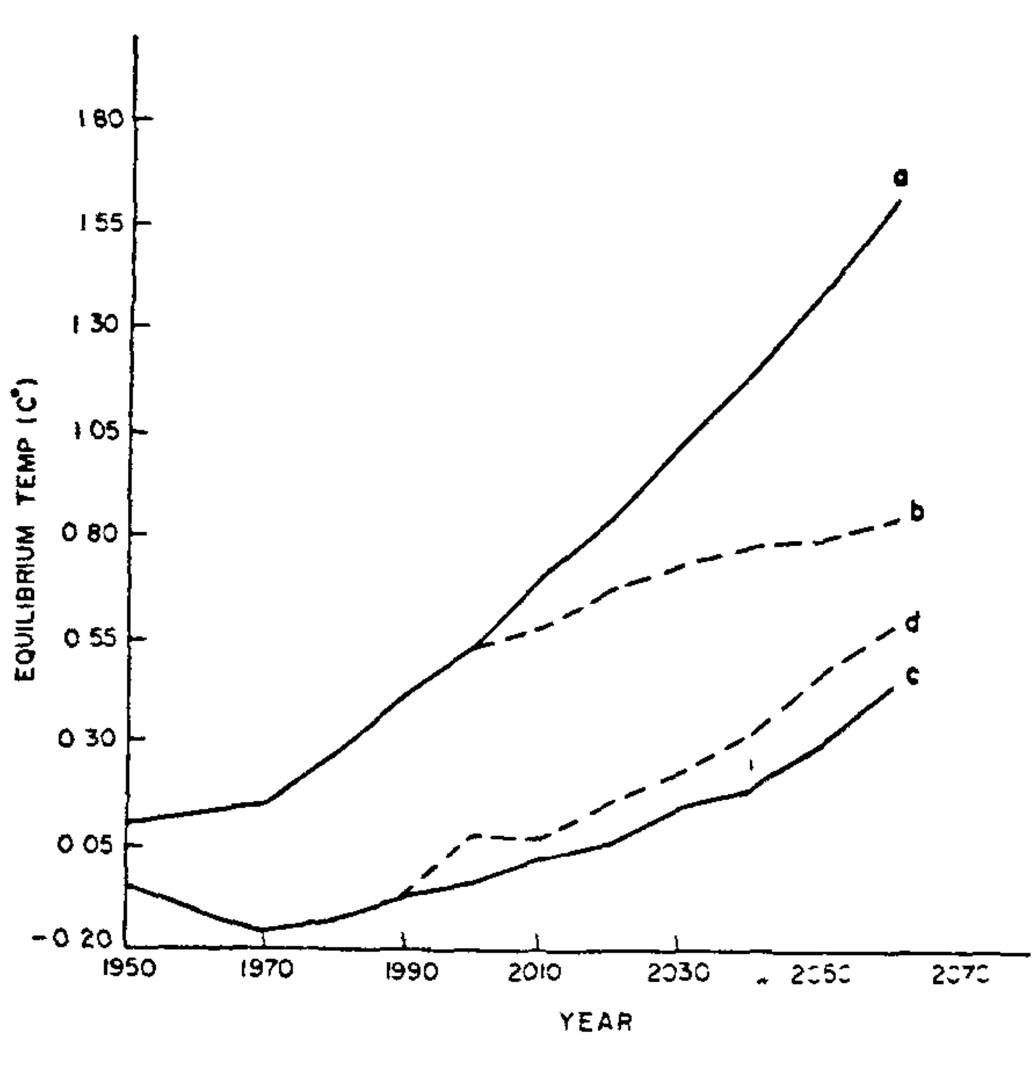

Figure 7. Equilibrium temperature change (°C) relative to preindustrial climate (1900) for the IPCC BaU scenario (curves a and c) and D scenario (curves b and d) Curves a and b are for CO_2 forcing and curves c and d are for the combined CO_2- and SO_2-induced total (direct and indirect) effect

warming by about 98% at the present time (1990) and 66% by the year 2060. An effort at levelling off and further reduction of the consumption of fuel will have smaller effect in offsetting the CO_2-induced warming, i e. about 27% by the year 2060. During the levelling-off phase, the positive forcing due to CO_2 will continue to grow whereas the aerosol forcing will remain constant, and during the decay (reduction) phase the positive forcing will start to level off and aerosol forcing will decline. These results will differ, however, if there is any characteristic change in fossil fuel use in future. For example, large-scale desulphurization (to reduce smog and acid rain) could enhance the warming due to increasing concentration of CO_2.

Even though annually and globally the averaged SO_2-induced forcing offsets CO_2-induced forcing to some extent, horizontal and vertical distributions of radiative forcing due to CO_2 and SO_2 are different. SO_2-induced forcing generally is regionally concentrated, with largest values occurring near the most prolific source of anthropogenic aerosols. The aerosol-induced cooling is expected to be larger in the NH because most of the emission sources are in the NH and because SO_2 and its products have a short lifetime. The regional pattern of indirect forcing is much more complicated than that of direct forcing. Still significant cooling occurs over the whole globe due to aerosol.

Our approach in estimation of climate change for future combinations of CO_2 and SO_2 emissions by combining the pattern for CO_2 alone and SO_2 alone appears to be justified, even though CO_2 and aerosol have different climate sensitivity. For example, the spatial correlation between the pattern of annual temperature change for combined CO_2 and aerosol forcing and the sum of the patterns for CO_2 alone and SO_2 alone is 0.86 (ref. 3).

There are some uncertainties concerning the relationship between the SO_2 emission and the CCN concentration and cloud optical thickness due to very restricted observational evidence. Also, global temperature records can be seriously affected by such perturbations as Mt. Pinatubo volcanic eruptions[25]. We thus need to improve our understanding of these processes. At present the distribution of sulphates globally is largely inferred from chemistry–transport models[26], rather than being directly measured.

1. Mitchell, J F. B , Manabe, S , Tokioka, T and Meleshko, V , *in Climate Change The IPCC Scientific Assessment* (eds Houghton, J T , Jenkins, G J And Ephraums, J J), Cambridge University Press, 1990, pp. 131–172
2 Gates, W L , Mitchell, J F B , Boer, G J , Cubasch, U and Meleshko, V , in *Climate Change· The IPCC Scientific Assessment* (eds Houghton, J T , Jenkins, G. J. and Ephraums, J J), Cambridge University Press, 1990, pp 97–134
3 Wigley, T. M L , *Nature*, 1994, **369**, 709–710
4 Charlson, R J , Langner, J and Rodhe, H , *Nature*, 1990, **348**, 22
5. Kiehl, J. T and Briegleb, B P., *Science*, 1993, **260**, 311–314
6 Taylor, K E. and Penner, J E , *Nature*, 1994, **369**, 734–737
7. Jones, A , Roberts, D L. and Slingo, A , *Nature*, 1994, **370**, 450–453
8 Wigley, T. M L., *Nature*, 1989, **339**, 355–357
9 Houghton, J T , Jenkins, G J and Ephraums, J J. (eds), *Climate Change: The IPCC Scientific Assessment*, Cambridge University Press, 1990, p 364

10 Kaufman, K. T. and Chou, M. D., *J. Climate*, 1993, **6**, 1241–1252
11 Moller, D., *Atmos. Environ*., 1984, **18**, 19–27
12 Whitby, K. T., *Atmos Environ*., 1978, **13**, 135–159
13 Twomey, S., *J Atmos Sci*., 1977, **34**, 1149–1152
14. Geleyn, J F and Hollingsworth, A., *Beitr Phys Atmos*., 1979, **52**, 1–16
15 Chou, M D and Arking, A., *J Atmos. Sci*., 1981, **38**, 798–807.
16 Lacis, A A and Hansen, J E., *J Atmos Sci*., 1974, **31**, 118–133
17. Fouquart, Y., in *Physically Based Modelling and Simulation of Climate and Climatic Change – Part I* (ed Schlesinger, M E), NATO Advanced Study Institute Series, 1987, pp 223–283
18 Stephens, G L., *J Atmos Sci*., 1978, **35**, 2123–2132
19 Starr, D O C. and Cox, S K., *J Atmos Sci*., 1985, **42**, 2682–2694
20 Chou, M D., *J Climate Appl Met*., 1986, **25**, 1532–1542
21 Chou, M D and Peng, L., *J Atmos Sci*., 1983, **25**, 1532–1542
22 Kneizys, F X, *et al*., Atmospheric Transmittance/Radiance Computer Code LOWTRAN 5, Optical Physics Div., 7670, HANSCOMAFB, Bedford, MA, 1980, p 23
23 Charlson, R J., Schwartz, S E., Hales, J M., Cess, R D., Coakley, Jr., J A., Hansen, J E. and Hofmann, D J., *Science*, 1992, **255**, 423–430
24 Manabe, S and Wetherald, R. J., *J Atmos Sci*., 1967, **32**, 3–15
25 Basett, Jr., G W and Lin, Z., *Climatic Change*, 1993, **25**, 179–184
26 Langner, J. and Rodhe, H., *J. Atmos Chem*., 1991, **13**, 225–263

ACKNOWLEDGEMENTS We are thankful to the Director General of Meteorology for kindly permitting us to send this paper to this journal We are thankful to Prof M. E. Schlesinger for kindly providing the University of Illinois multilayer radiative–convective model for our calculations.

Received 5 December 1994; revised accepted 26 April 1995

Magnetic polarity stratigraphy of the Pinjor Formation (Upper Siwalik) near Pinjore, Haryana

A. Ranga Rao*, A. C. Nanda*, U. N. Sharma and M. S. Bhalla†**

*Wadia Institute of Himalayan Geology, Dehra Dun 248 007, India, **Oil and Natural Gas Corporation Ltd., Nazira, India, †National Geophysical Research Institute, Hyderabad 500 007, India

The magnetostratigraphic and vertebrate faunal studies were carried out in the type section of the Pinjor Formation (Pinjor Faunal Zone of Pilgrim[1]) near Pinjore township, Haryana. The Patiali Rao section exposes both Pinjor and pre-Pinjor beds with a thickness of 1296 m. Oriented samples were collected from 52 sites. The data permit one to conclude that the type Pinjor Faunal Zone of Pilgrim covers the entire Matuyama reverse chron and lower part of Bruhnes normal chron with a time span from 2.47–0.63 Ma. Fresh vertebrate fossil collection indicates that the Pinjor Faunal Zone is marked by the first appearance of *Equus, Cervus* and *Leptobos*.

IT is now established that 'faunal zones' of Pilgrim[1] are very vaguely defined and their boundaries can neither be located in the field nor be used in mapping. For this reason ONGC workers[2] subdivided the outcropping sequence on lithological basis for purposes of mapping. In the vicinity of Chandigarh, they divided the Upper Siwalik sequence into five lithounits and designated the basal part as 'Masol Formation' overlain successively by Rupar I, II, III and IV formations. The subdivision of the Rupar Formation is based on the presence of pebble beds. The Masol Formation was correlated on faunal evidences to the Tatrot Faunal Zone and Rupar I, II and III to the Pinjor Faunal Zone of Pilgrim[1]. The conglomeratic facies of the Rupar IV was correlated to the Boulder Conglomerate. Present investigations are confined to a section along stream, locally known as Patiali Rao, which is a part of the type area of the Pinjor Faunal Zone of Pilgrim[1]. Patiali Rao section exposes 1296 m of sediments. Vertebrate fossils were collected, identified and clubbed with the magnetostratigraphic studies. The geological map of the area is given in Figure 1.

Not much data on the magnetostratigraphic studies of the Upper Siwalik subgroup are available from India. However, studies were conducted in the Chandigarh region by Yakoyama[3], Azzaroli and Napoleone[4] and Tandon *et al.*[5]. Ranga Rao *et al.*[6] carried out magnetostratigraphic studies in the Upper Siwalik sequence exposed in the vicinity of Jammu Hills. Ranga Rao[7] synthesized the magnetostratigraphic data of various Siwalik sections.

Faunal findings in Pinjore area

Sahni and Khan[8] carried out stratigraphic and vertebrate palaeontologic studies of the area lying east of Chandigarh, including Patiali Rao section. Later, Badam[9] and Gaur[10] also made collections, but Sahni and Khan's work formed the base. On the basis of fauna as well as lithology Sahni and Khan[8] for the first time recognized pre-Pinjor or the Tatrot beds (= Masol Formation of ONGC) and Lower Boulder Conglomerate (Rupar IV of ONGC). They further identified about 80 m thick succession, characterized mainly by grey clays towards the top of the Tatrot Formation which yielded rich vertebrate fossils (yielding 98% of their fossil collection), and named it as 'Quaranwala Zone'. This zone was